Three-nucleon force effects in inclusive spectra of the neutron-deuteron breakup reaction

H. Witała,* J. Golak, R. Skibiński, V. Soloviov, and K. Topolnicki
M. Smoluchowski Institute of Physics, Jagiellonian University, PL-30348 Kraków, Poland

(Received 21 February 2020; accepted 14 May 2020; published 28 May 2020)

We investigate the sensitivity of the nonexclusive nucleon induced deuteron breakup reaction to the three-nucleon interaction and distributions of three-nucleon force effects in inclusive spectra. To this end we solve the three-nucleon Faddeev equation at a number of incoming nucleon laboratory energies using the CD Bonn nucleon-nucleon interaction alone or combined with the 2π-exchange Tucson-Melbourne three-nucleon force. Based on these solutions, energy spectra of an outgoing nucleon, at a specified detection angle as well as spectra integrated over that angle, are calculated. By integrating the spectra at a given angle over the energy of the outgoing nucleon the angular distributions of three-nucleon force effects in the breakup process are additionally obtained. Contrary to elastic nucleon-deuteron scattering, where at higher energies significant three-nucleon force effects were encountered for scattering angles around the minimum of the cross section, for the breakup process only moderate effects are found and they are restricted to forward angles. Results of the present investigation show that the large three-nucleon force effects found for some specific complete breakup configurations are reduced substantially in the incomplete spectra when averaging over contributing complete geometries is performed.

DOI: 10.1103/PhysRevC.101.054002

I. INTRODUCTION

Studies of the three-nucleon ($3N$) continuum revealed significant three-nucleon force (3NF) effects in the elastic nucleon-deuteron (Nd) scattering and the deuteron breakup reactions. Namely, for laboratory energies of the incoming nucleon above $\approx$60 MeV large discrepancies between theoretical predictions and data were found in the angular distributions of the elastic Nd scattering observables [1–3] as well as in the total cross section for neutron-deuteron (nd) scattering [4,5]. Also in some kinematically complete breakup configurations large changes of the cross section caused by 3NF's were predicted [6]. Generally the detected 3NF effects grow with the increasing energy of the incoming nucleon. The commonly used (semi)phenomenological long-range 2π-exchange 3NF's, such as the Tucson-Melbourne (TM) [7] or the Urbana IX [8] when combined with (semi)phenomenological, high-precision nucleon-nucleon (NN) potentials, such as the AV18 [9], the CD Bonn [10], the Nijm1 or the Nijm2 [11] forces are able to explain the dominant part of the discrepancy for the incoming nucleon energies up to about 135 MeV. However, at still higher energies a significant part of the deviation from data remains unexplained [2,5]. Since the relativistic $3N$ Faddeev calculations [12,13] showed only negligible effects of relativity for the elastic scattering observables and the total nd cross section at energies up to the π production threshold, therefore those remaining discrepancies indicate the action of short-range components of the 3NF absent in the above-mentioned models.

Since the total cross section for nd scattering is a sum of the total elastic scattering and breakup cross sections, interesting questions arise about importance of 3NF effects in incomplete spectra of the breakup process as well as on their distribution and dependence on the incoming neutron energy. To answer them we investigated, at a number of incoming neutron energies, in the range 14–294 MeV, the energy spectra of the outgoing nucleon, taken as a proton or a neutron, in the incomplete breakup. We examined energy spectra at a specific laboratory angle of the outgoing nucleon as well as the energy spectra arising from integrations over this angle. Integrating the energy spectra at a specific angle of the outgoing nucleon over the allowed nucleon energy enabled us to determine angular distributions of the single-nucleon inclusive breakup cross sections. It permitted us to determine how 3NF effects are spread over the angular domain in incomplete breakup and to compare it to the angular distribution of 3NF effects in the elastic nd scattering.

The paper is organized as follows. In Sec. II we describe briefly the underlying theoretical formalism leading to predictions for different energy spectra. We present and discuss our results in Sec. III. Finally, we summarize and conclude in Sec. IV.

II. SINGLE-NUCLEON ENERGY SPECTRA AND ANGULAR DISTRIBUTIONS IN THE DEUTERON BREAKUP REACTION

Neutron-deuteron scattering with the nucleons interacting through a nucleon-nucleon potential v_{NN} and a three-nucleon

*henryk.witala@uj.edu.pl

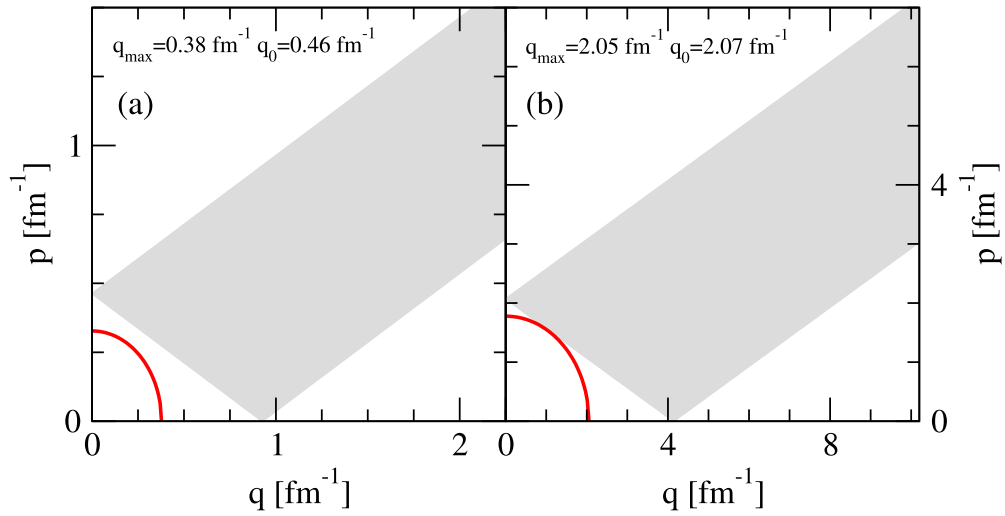

FIG. 1. Regions in the (q-p) plane (see text) which contribute to the breakup reaction (red solid line) and to the $\langle\phi'|PT|\phi\rangle$ term of the elastic scattering amplitude (gray highlighted region) at the incoming nucleon laboratory energy $E = 10$ (a) and 200 MeV (b).

force $V_4 = V_4^{(1)} + V_4^{(2)} + V_4^{(3)}$ is described in terms of the breakup operator T satisfying the Faddeev-type integral equation [14–17]

$$T|\phi\rangle = tP|\phi\rangle + (1+tG_0)V_4^{(1)}(1+P)|\phi\rangle + tPG_0T|\phi\rangle + (1+tG_0)V_4^{(1)}(1+P)G_0T|\phi\rangle. \quad (1)$$

The two-nucleon t-matrix t is the solution of the Lippmann-Schwinger equation with the interaction v_{NN}. The permutation operator $P = P_{12}P_{23} + P_{13}P_{23}$ is given in terms of the transposition operators, P_{ij}, which interchange nucleons i and j. The incoming state $|\phi\rangle = |\vec{q}_0\rangle|\varphi_d\rangle$ describes the free nucleon-deuteron motion with relative momentum $\vec{q}_0$ and the deuteron wave function $|\varphi_d\rangle$. Finally, G_0 is the resolvent of the three-body center of mass kinetic energy. Each $V_4^{(i)}$ part of 3NF is symmetric under the exchange of the nucleons j and k ($i, j, k = 1, 2, 3$ and $j \neq i \neq k \neq j$).

The transition amplitudes for the elastic nd scattering, $\langle\phi'|U|\phi\rangle$, and breakup reactions, $\langle\phi_0|U_0|\phi\rangle$, are given in terms of T by [14–17]

$$\begin{aligned}\langle\phi'|U|\phi\rangle &= \langle\phi'|PG_0^{-1} + V_4^{(1)}(1+P) + PT \\ &\quad + V_4^{(1)}(1+P)G_0T|\phi\rangle, \\ \langle\phi_0|U_0|\phi\rangle &= \langle\phi_0|(1+P)T|\phi\rangle. \end{aligned} \quad (2)$$

In the latter case the transition amplitude comprises a final breakup state $|\phi_0\rangle = |\vec{p}_1\vec{q}_1 m_1 m_2 m_3\rangle$ of three outgoing nucleons defined by individual nucleon spin projections m_i and by two relative Jacobi momenta $\vec{p}_1$ and $\vec{q}_1$, which are linear combinations of the individual nucleon momenta $\vec{k}_i$:

$$\begin{aligned}\vec{p}_i &= \tfrac{1}{2}(\vec{k}_j - \vec{k}_k), \\ \vec{q}_i &= \tfrac{2}{3}\left[\vec{k}_i - \tfrac{1}{2}(\vec{k}_j + \vec{k}_k)\right], \end{aligned} \quad (3)$$

for $\{i, j, k\} = \{1, 2, 3\}$ and cyclic permutations. The center-of-mass energy of the $3N$ system $E_{\rm c.m.}$ is specified by incoming relative nucleon-deuteron momentum $\vec{q}_0$ and the deuteron binding energy E_d:

$$E_{\rm c.m.} = \frac{3}{4m}q_0^2 + E_d \equiv \frac{3}{4m}q_{\rm max}^2 = \frac{3}{4m}q_i^2 + \frac{1}{m}p_i^2, \quad (4)$$

where m is the nucleon mass.

It follows from Eq. (2) that contributions to a particular kinematically complete breakup configuration, specified by momenta of three outgoing nucleons, are given by three matrix elements $\langle\vec{p}_i\vec{q}_i m_1 m_2 m_3|T|\phi\rangle$ determined at three pairs of momentum magnitudes (p_i, q_i) lying on an ellipse in the (q-p) plane, given by Eq. (4) (see Fig. 1). Performing exclusive or inclusive breakup measurements one is restricted to points lying on that ellipse. While the exclusive breakup is very selective, being restricted to only three (p_i, q_i) points, in the incomplete breakup one integrates over contributing complete geometries along that curve. Thus the incomplete breakup delivers information on the underlying dynamics averaged over configurations which are taken into account. In contrast to the breakup reaction, the elastic Nd scattering receives contributions from practically all regions of the (q-p) plane, due to the integration over the relative momentum of the two nucleons forming the deuteron. It is interesting to note that the region of the (q-p) plane which contributes to the elastic scattering transition amplitude by the dominant $\langle\phi'|PT|\phi\rangle$ term does not overlap with the ellipse of contributions to the breakup reaction. Namely, contributions of that term to elastic nd scattering come from the region of (q, p) values with $p \in (|q_0 - \frac{1}{2}q|, q_0 + \frac{1}{2}q)$ (see the Appendix). In Fig. 1 we exemplify that separation of breakup and elastic scattering regions of the (q-p) plane for two laboratory energies of the incoming neutron: $E = 10$ and 200 MeV.

It follows that the sensitivity of breakup observables to the underlying dynamics, in particular their sensitivity to 3NF effects, will be different from the sensitivity of the elastic Nd scattering observables. Also the averaging over many contributing kinematically complete geometries, should reduce sensitivity of the incomplete breakup to the underlying dynamics.

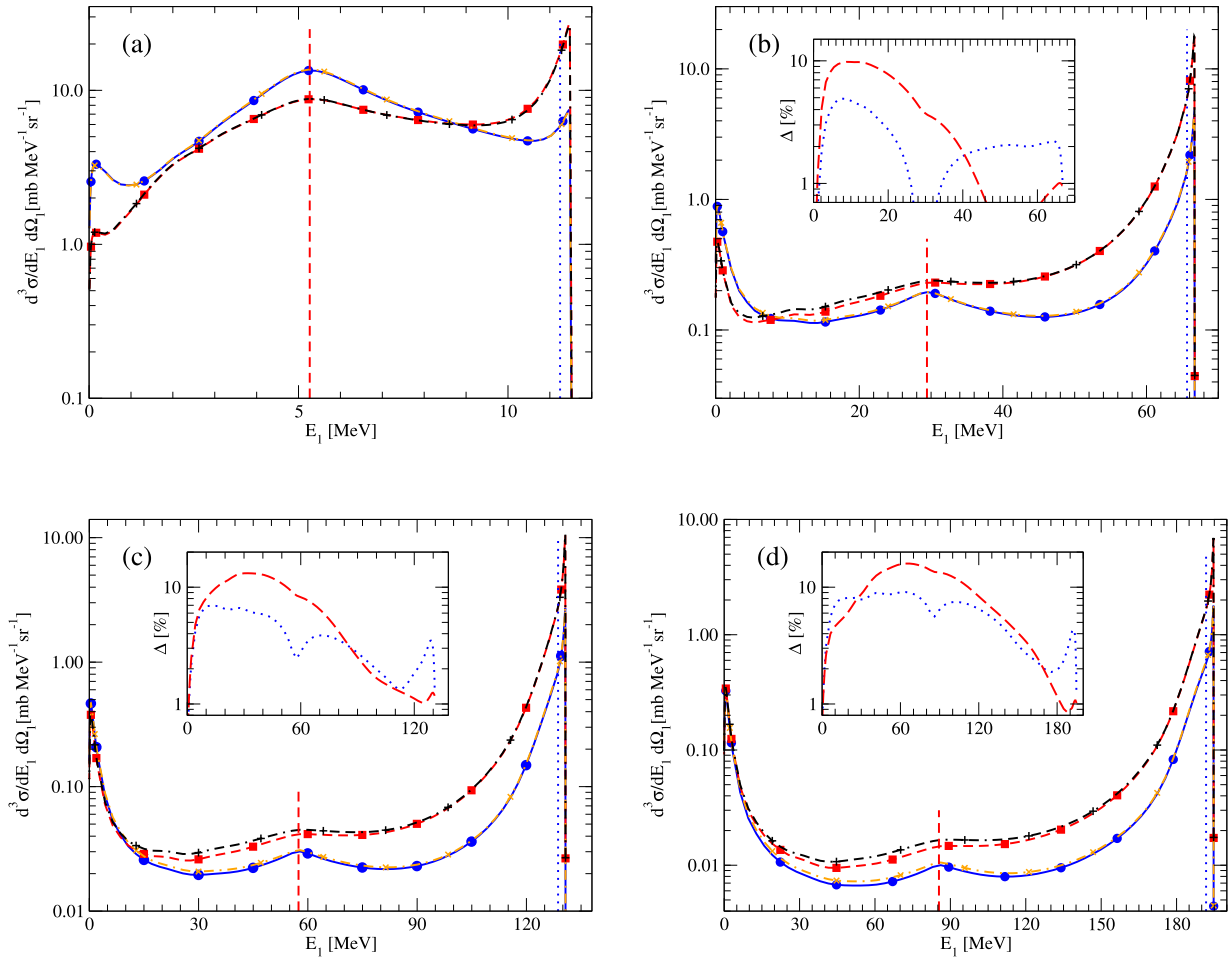

FIG. 2. The threefold differential cross section $\frac{d^3\sigma}{d\Omega_1 dE_1}$ of the outgoing nucleon detected at the laboratory angle $\theta_1^{\rm lab} = 10^\circ$ in the $d(n, N_1)N_2N_3$ breakup reaction for the laboratory energy of the incoming neutron $E = 14$ (a), 70 (b), 135 (c), and 200 (d) MeV. The spectra of the outgoing neutron in the $d(n, n)np$ reaction are shown with the (blue) solid line, marked with circles when nucleons interact with the CD Bonn potential only. Combining the CD Bonn with the TM99 3NF gives the (orange) dashed-dotted line, marked with an "x". The spectra of the outgoing proton are given by the (red) dashed line, marked with squares, (the CD Bonn only) and the (black) double-dashed-dotted line, marked with pluses, (the CD Bonn +TM99). The position of QFS(1-2) and QFS(1-3) is given by the (blue) dotted vertical line. The position of FSI(1-2) and FSI(1-3) is given by the (red) dashed vertical line. In inserts the magnitudes of 3NF effects defined by $\Delta \equiv \frac{\sigma(NN+3{\rm NF})-\sigma(NN)}{\sigma(NN)} \times 100\%$ are shown with the (blue) dotted line for the outgoing neutron and with the (red) long-dashed line for the outgoing proton.

The reduction of sensitivity will depend on the complete configurations over which the averaging is done. Performing a standard incomplete breakup measurement one outgoing nucleon is detected at a specific laboratory angle and its energy spectrum is measured. In other conceivable incomplete measurements the energy spectrum of the outgoing nucleon stemming from some angular range can be determined. Both types of energy spectra can be predicted theoretically by performing proper integrations over the Jacobi momenta of the contributing complete configurations. Integration of the energy spectra at a specific angle over an energy of the outgoing nucleon provides the angular distribution of the incomplete breakup.

In order to investigate the sensitivity of such various spectra to the 3NF and to compare them with elastic nd scattering we solved the 3N Faddeev equation in a partial wave momentum-space basis for a number of the incoming nucleon laboratory energies $E = 14, 70, 100, 135, 200, 250,$ and 294 MeV. As a NN interaction we used the high precision semiphenomenological CD Bonn potential [10]. We took that interaction alone or together with the TM99 3NF [7] whose cut-off parameter Λ was adjusted so that this particular combination of a NN and 3N force reproduced the experimental triton binding energy [2]. When solving the 3N Faddeev equation we included all 3N partial wave states with the total two-nucleon angular momentum $j \leqslant 5$ and the total 3N angular momentum $J \leqslant 25/2$.

III. RESULTS AND DISCUSSION

In Fig. 2 we show the threefold differential cross section $\frac{d^3\sigma}{d\Omega_1 dE_1}$ as a function of the energy E_1. Specifically, in Fig. 2 the energy spectra of the outgoing nucleon (neutron or proton) from incomplete breakup $d(n, N_1)N_2N_3$, detected at a laboratory angle $\theta_1^{\rm lab} = 10^\circ$ are exemplified at four incoming neutron laboratory energies $E = 14, 70, 135,$ and 200 MeV.

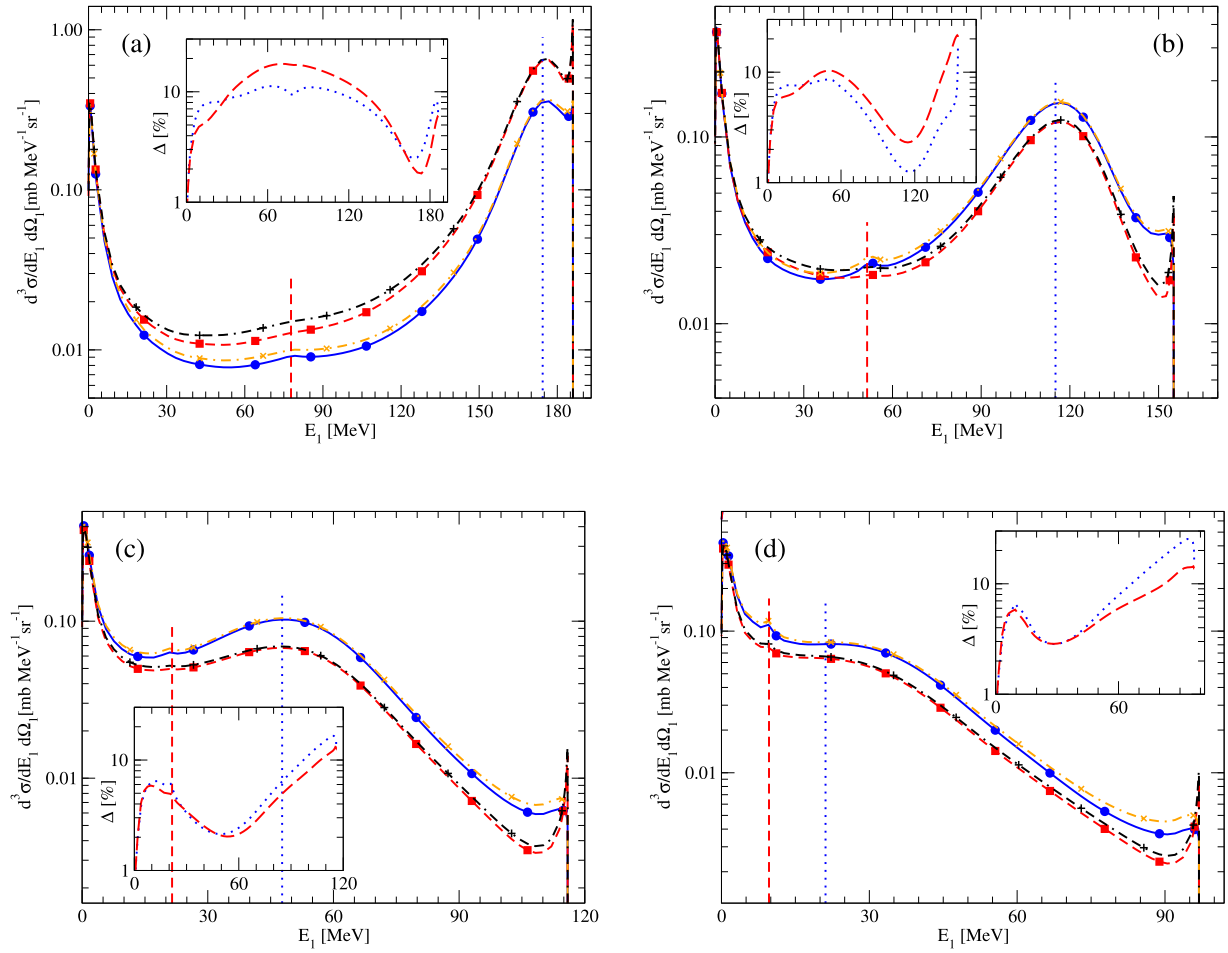

FIG. 3. The energy spectra $\frac{d^3\sigma}{d\Omega_1 dE_1}$ of the outgoing nucleon at the laboratory angles $\theta_1^{\rm lab} = 20^\circ$ (a), 40° (b), 60° (c), and 70° (d) in the $d(n, N_1)N_2N_3$ breakup reaction for the laboratory energy of the incoming neutron $E = 200$ MeV. For description of lines and inserts see Fig. 2.

These spectra unveil a characteristic structure, with a peak at the highest energy of the outgoing nucleon, which is due to a strong final state interaction of nucleons 2 and 3 [FSI(2-3)], having a small relative energy, in a nucleon-nucleon partial wave state $^1S_0$. The enhancement of the cross section in the region of vanishing energy of nucleon 1 results from approaching the quasifree scattering (QFS) complete breakup geometry defined by the condition $\vec{p}_1 = 0$. That QFS configuration corresponds to quasifree scattering of nucleons 2 and 3 [QFS(2-3)]. In the spectra one can see also two additional dominating contributions coming from specific kinematically complete breakup configurations with large cross sections, whose positions are indicated by vertical dotted and dashed lines. One of them is QFS(1-2) ($\vec{p}_3 = 0$) and QFS(1-3) ($\vec{p}_2 = 0$) occurring at E_1 indicated by the (blue) dotted vertical line, and appearing in the energy spectrum at laboratory angles of nucleon 1 below some angle $\theta_1^{\rm max}$ given in terms of the incoming neutron laboratory energy E and the deuteron binding energy E_d by $\theta_1^{\rm max} = \arcsin(\sqrt{-\frac{2E_d}{E}})$. The second dominating contribution comes from the kinematically complete breakup geometry FSI(1-2) (kinematical condition $\vec{p}_1 = \vec{p}_2$) and FSI(1-3) ($\vec{p}_1 = \vec{p}_3$), which occurs at E_1 indicated by a (red) vertical dashed line, and appears in the energy spectrum up to a laboratory angle $\theta_1^{\rm max} = \arcsin(\sqrt{-\frac{3E_d}{2E}})$. These positions move when changing the angle of the outgoing nucleon, what is exemplified in Fig. 3 at the incoming energy $E = 200$ MeV and four angles $\theta_1^{\rm lab} = 20^\circ, 40^\circ, 60^\circ$, and 70°.

While the structure of the threefold differential cross section for the outgoing neutron at given θ_1 is similar to that of the outgoing proton, the behavior of the incomplete cross section with respect to the energy and detection angle depends on the isospin projection of the detected particle. For example at $E = 200$ MeV (see Figs. 2 and 3) the neutron energy spectrum at forward angles lies below the proton one but with the increasing angle it overshoots the proton spectrum. The 3NF effects start to appear at $E = 70$ MeV (see Fig. 2), similarly as in the elastic Nd scattering process. At forward angles (10°) they are concentrated at the lower part of the spectrum where they enhance the cross section predicted with NN potential only. At 70 MeV they change the cross section by up to 10%, strengthening this effect to $\approx$20% at 200 MeV. With the increasing detection angle the region of significant changes of the cross section extends to higher energies E_1. At larger angles and energies the magnitude of the cross section is however reduced by a factor of about 10.

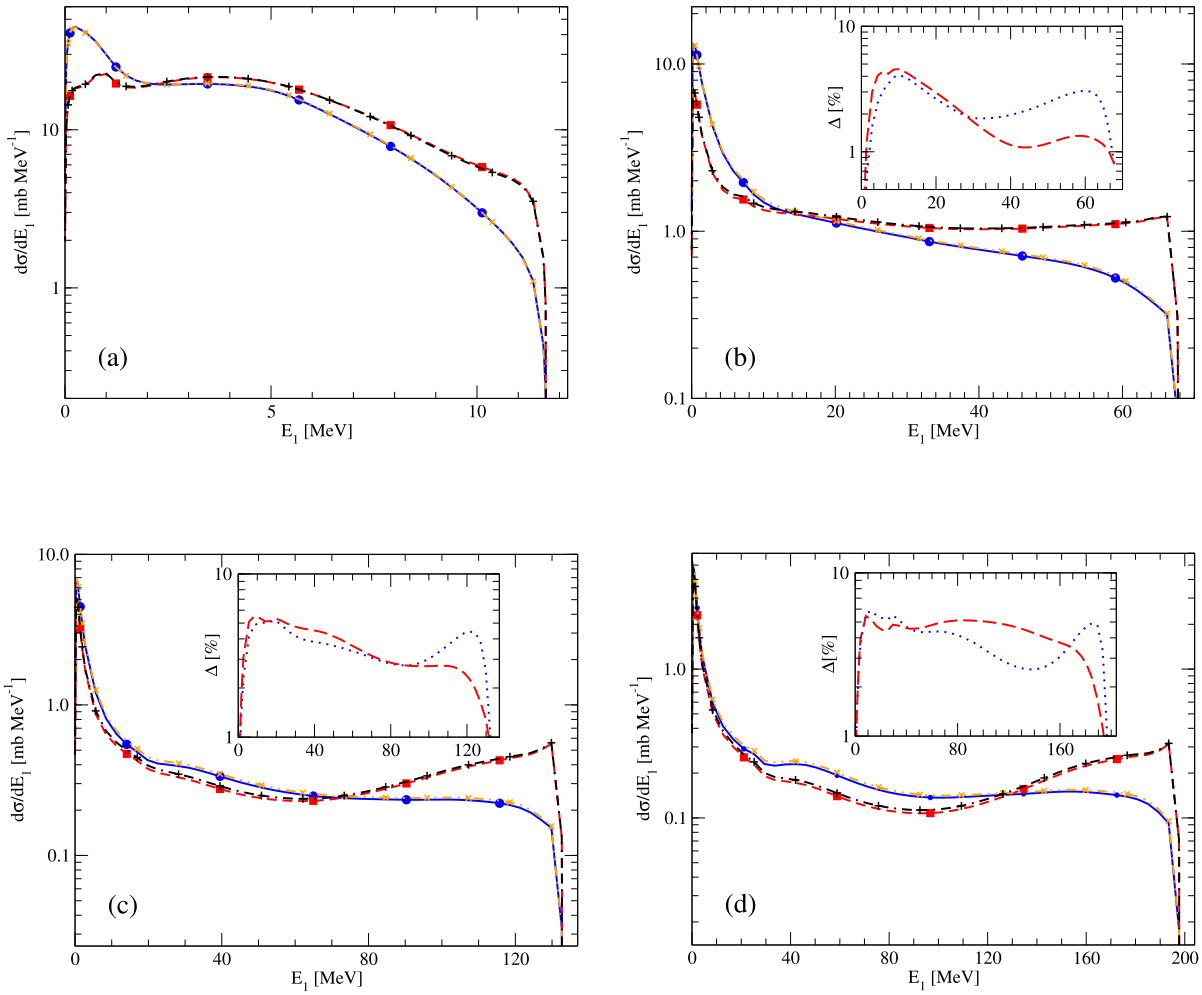

FIG. 4. The angle-integrated energy spectra $\frac{d\sigma}{dE_1}$ of the outgoing nucleon in the $d(n, N_1)N_2N_3$ breakup reaction for the laboratory energy of the incoming neutron $E = 14$ (a), 70 (b), 135 (c), and 200 (d) MeV. The spectra of the outgoing neutron in the $d(n, n)np$ reaction are given with the (blue) solid line, marked with circles when nucleons interact with the CD Bonn potential only. Combining the CD Bonn with the TM99 3NF gives the (orange) dashed-double-dotted line, marked with an "x". The spectra of the outgoing proton are given by the (red) dashed line, marked with squares (the CD Bonn only), and the (black) double-dashed-dotted line, marked with pluses, (the CD Bonn + TM99). For explanation of inserts see Fig. 2.

This behavior of the cross section together with the distributions of the 3NF effects are reflected in the angle-integrated energy spectra, $\frac{d\sigma}{dE_1}$, shown in Fig. 4. The angular integration reduces contributions from the threefold differential cross section at forward angles with large 3NF effects, leading to the angle-integrated energy spectra with 3NF effects distributed more or less uniformly along the spectrum with the magnitude of effects changing from ≈2–3% at 70 MeV to ≈4–6 % at 200 MeV. A reduction of 3NF effects when going from the spectra at given angle to angle integrated spectra exemplifies a reduction of sensitivity of the incomplete breakup due to averaging over contributing complete geometries. While for complete breakup in specific configurations 3NF effects of a magnitude up to ≈90% were found at 200 MeV [6], in the energy spectra at a specific angle of the outgoing nucleon they diminish to ≈20% and reduce further to ≈6% when additional integration over the angle is performed. One can expect that further averaging by performing integrations over the energy of the outgoing nucleon would lead to even smaller 3NF effects in the total breakup cross section.

To investigate that issue we studied the angular distributions of the incomplete breakup cross sections and compared them to the ones in elastic *nd* scattering. The spectra at a specific angle integrated over energy of the outgoing nucleon are shown in Fig. 5 as functions of the laboratory angle of the detected nucleon. In this figure also the laboratory angular distributions of the cross section for elastic *nd* scattering are presented together with magnitudes of 3NF effects for both elastic scattering and the breakup reaction shown in inserts of that figure. The 3NF effects in the breakup, contrary to elastic scattering, are restricted to the angles below ≈120° and are similar in magnitude for the detected neutron or proton. At 70 MeV effects are ≈2–3% up to about $\theta_1^{\rm lab} \approx 100°$, at 135 MeV ≈3–4 % up to $\theta_1^{\rm lab} \approx 120°$, and at 200 MeV ≈4–5 % up to $\theta_1^{\rm lab} \approx 110°$. With the increasing energy they extend to bigger angles and at 200 MeV they reach ≈2%

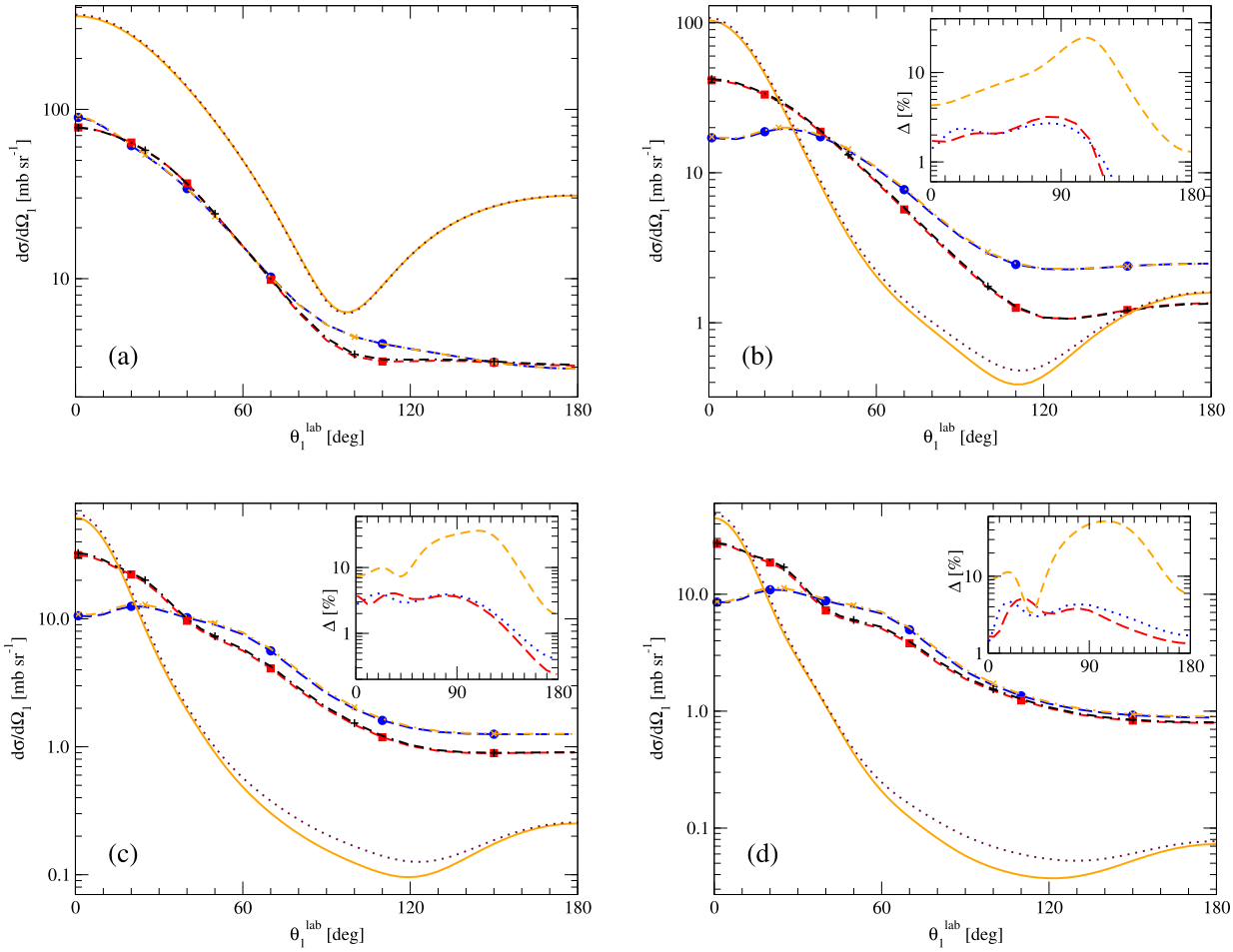

FIG. 5. The energy spectra from Fig. 2 integrated over the energy of the outgoing nucleon shown as a function of the laboratory angle of that nucleon. The incoming nucleon kinetic energy in the laboratory system is $E = 14$ (a), 70 (b), 135 (c), and 200 (d) MeV. The angular distribution of the outgoing neutron in the $d(n, n)np$ reaction is given with the (blue) dashed line, marked with circles when nucleons interact with the CD Bonn potential only. Combining the CD Bonn with the TM99 3NF gives the (orange) dashed-double-dotted line, marked with "x". The angular distribution of the outgoing proton is given by the (red) dashed line, marked with squares, (the CD Bonn only) and the (black) double-dashed-dotted line, marked with pluses, (the CD Bonn + TM99). The laboratory angular distributions for the elastic nd scattering is given by the (orange) solid line (the CD Bonn only) and the (maroon) dotted line (te CD Bonn + TM99). For explanation of inserts see Fig. 2. In inserts shown here the additional (orange) short-dashed line represents the magnitude of 3NF effects for elastic nd scattering as defined in caption to Fig. 2.

for $\theta_1^{\rm lab} \approx 150^\circ$. The 3NF effects in the angular distributions of the breakup process are significantly smaller than those in elastic *Nd* scattering, where at 200 MeV they amount to ≈50% in the region of the cross section minimum (see Fig. 5).

In Fig. 6(a) we show, as functions of the laboratory energy E of the incoming neutron, the total *nd* cross section data from Ref. [4] together with the CD Bonn and the CD Bonn + TM99 based theoretical predictions. Similarly to the elastic scattering angular distributions of the cross sections, 3NF effects start to appear in the total *nd* cross section at about 60 MeV. Standard models of 3NF such as the TM99 or the UrbanaIX are able to explain the difference between the total *nd* cross section data and theoretical predictions based on *NN* potentials up to ≈135 MeV [4,5]. At higher energies, however, they fail to reproduce the total cross section data, leaving a significant deviation to data which is rapidly growing with the energy, as exemplified in Fig. 6(a) for the CD Bonn *NN* potential and the TM99 3NF model.

The elastic scattering and breakup total cross sections predicted by the CD Bonn potential alone or combined with the TM99 3NF force are shown in Fig. 6(b). Since the angular distributions of the cross sections for breakup and elastic scattering are peaked at forward angles (see Fig. 5), the magnitude of 3NF effects as given by the TM99 model for the total *nd* breakup and total elastic scattering cross sections can be traced back to the angular distributions of 3NF effects in these processes. A uniform distribution of 3NF effects in the region of angles with large breakup cross sections leads to a magnitude of 3NF effects of ≈2–3 % for the total *nd* breakup cross section (see Fig. 6(c)). The main region of large 3NF effects for elastic scattering is located around the minimum of the cross section, therefore the magnitude of 3NF effects in the total elastic scattering cross section is reduced to ≈6–10 %

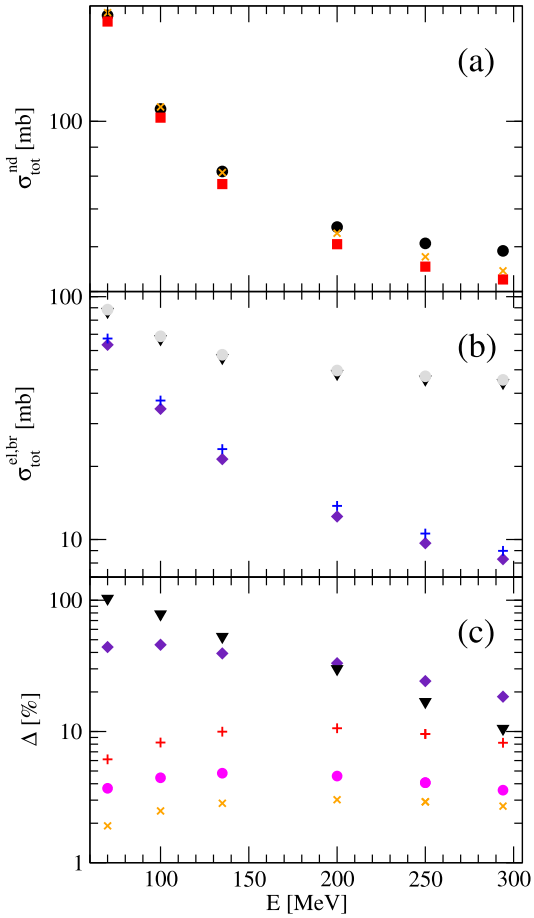

FIG. 6. The total cross section for *nd* scattering (a) and the total *nd* elastic scattering and the total breakup cross sections (b) as functions of the laboratory energy E of the incoming neutron. In (a) (black) dots demote experimental total cross section data from Ref. [4] and (red) squares and (orange) exes represent the CD Bonn and the CD Bonn + TM99 based total *nd* cross section predictions, respectively. In (b) the corresponding predictions for the total elastic scattering cross sections are given by (indigo) diamonds and (blue) pluses, while for the total breakup cross section by (black) triangles and (grey) dots. In (c) the contributions from the elastic scattering and breakup reactions provided by the TM99 3NF to the difference between the experimental total nd cross section and its prediction by the CD Bonn potential only, defined by $\Delta \equiv \frac{\sigma_{el,br}^{tot,NN+3NF} - \sigma_{el,br}^{tot,NN}}{\sigma_{exp}^{tot} - \sigma^{tot,NN}} \times 100\%$, are shown by (indigo) diamonds for elastic scattering and by (black) triangles for breakup contribution. The (magenta) dots, (red) pluses, and (orange) exes show the magnitude of the TM99 3NF effects, defined by $\Delta \equiv \frac{\sigma_{tot,el,br}^{tot,NN+3NF} - \sigma_{tot,el,br}^{tot,NN}}{\sigma_{tot,el,br}^{tot,NN}} \times 100\%$, for the total *nd* cross section, as well as for the elastic scattering and breakup total cross sections, respectively.

(see Fig. 6(c)). For energies above ≈70 MeV the dominating contribution to the total cross section comes from the breakup reaction as shown in Fig. 6(b) (see also Ref. [6]), which results in the magnitude of 3NF effects in the total *nd* cross section being of the order of ≈4% for energies above 70 MeV.

It is also interesting to study contributions to the difference between the total *nd* cross section data and the CD Bonn potential prediction which are induced by the TM99 3NF and which come from elastic scattering and breakup processes separately. They are shown in Fig. 6(c) by diamonds for the elastic scattering and by triangles for the breakup contributions. At 200 MeV the TM99 3NF explains ≈60% of that difference with approximately equal contributions from the elastic scattering and breakup reactions. At 250 MeV only ≈45% is explained with ≈25% and ≈20% contributions from the elastic scattering and breakup processes, respectively. At 294 MeV the explained part reduces further to only ≈30% with contributions of ≈20% from the elastic scattering and ≈10% from the breakup reaction.

It is clear that in order to explain the total *nd* cross section data at energies around ≈200 MeV a 3NF model containing only long-range 2π-exchange mechanism is not sufficient. The rapid growth of the unexplained part of the total cross section with increasing energy indicates that the mechanism responsible for it must provide contributions that also quickly increase with the energy. Among possible mechanisms one could consider short-range components of the 3NF modelled by the π-ρ or ρ-ρ 3NF's [18] exchanges or the corresponding short-range components of 3NF as provided in the framework of the chiral perturbation theory [19–23]. The unexplained part of the total cross section shows that, in spite of the substantial reduction of the 3NF effects due to averaging over contributing exclusive geometries in incomplete breakup, the experimental data for such averaged breakup observables, comprising in addition to incomplete spectra also information about the total breakup cross section, are desirable. Due to the dominating contribution of the breakup reaction to the total cross section at higher energies such data would help to resolve the total cross section discrepancy by exhibiting the role played by 3NF, specifically by its short-range components. The well-established 3NF effects in the region of the minimum of the elastic *nd* scattering cross section contribute only slightly to that discrepancy. Namely, at $E = 250$ MeV, where elastic *nd* scattering data are available, the part of the elastic scattering cross section data in the region of c.m. angles $60^\circ \lesssim \theta_{c.m.} \lesssim 180^\circ$ unexplained by inclusion of the 2π-exchange 3NF, provides only ≈7% contribution to the unexplained by the 2π-exchange 3NF part of the total cross section at that energy. This demonstrates the importance of the breakup studies for resolving the total cross section discrepancy and makes it plausible that the magnitude of contributions from short-range components of the 3NF should be at higher energies at least as large as the ones stemming from the 2π-exchange mechanism.

IV. SUMMARY AND CONCLUSIONS

We investigated the magnitudes and the distributions of 3NF effects in incomplete *nd* breakup based on solutions of the 3*N* Faddeev equation with the CD Bonn potential alone or augmented with the TM99 3NF. Energy spectra of the outgoing neutron or proton were calculated either at a specific laboratory angle of the outgoing nucleon or by integrating over some angular range. The spectra at a specific angle (the threefold differential cross sections) reveal structures caused by dominant contributing kinematically complete

configurations such as FSI or QFS. The 3NF effects start to appear at ≈60 MeV of the incoming neutron laboratory energy. At forward angles large 3NF effects are located in the lower parts of the spectra, shifting to larger outgoing nucleon energies with increasing angle. Integration of the threefold differential cross section given at a specific angle over the outgoing nucleon energy leads to the angular distributions of the breakup cross section for single-nucleon detection, which is different from the angular distribution of the corresponding elastic scattering cross section. In contrast to elastic scattering, where the interference between the direct PT and exchange PG_0^{-1} terms leads to a characteristic minimum of the cross section, the angular distribution of the breakup reaction is peaked at forward angles and recedes with the increasing angle. Additionally, the largest 3NF effects are localized being uniformly spread at forward angles, as opposed to elastic scattering, where they are dominant in the region of the minimum of the elastic scattering cross section. The long-ranged 2π-exchange TM99 3NF is unable to explain the angular distributions of the elastic scattering cross section as well as the total nd cross section data at higher energies. The difference between the nd total cross section data and the theoretical predictions which include the 2π-exchange TM99 3NF grows rapidly with the increasing energy of the incoming nucleon, which indicates that the short-range components of the 3NF can be responsible for this discrepancy. Such short-range forces could probably provide contributions quickly increasing with the energy and dominating at higher energies. It will be interesting to examine if short-range components of the 3NF which are consistently derived in the framework of chiral effective field theory are able to describe the total nd cross section data.

The presented inclusive spectra for the deuteron breakup process reveal smaller $3N$ force effects than those observed in some exclusive geometries. Thus, to determine the structure and importance of $3N$ interaction exclusive measurements would seem to be preferable. However, the complete breakup cross sections in configurations with large $3N$ force effects become hardly measurable at increasing beam energies, so the inclusive experiments, which provide supplementary information, are necessary to study properties of the $3N$ potential.

ACKNOWLEDGMENTS

This study has been performed within the Low Energy Nuclear Physics International Collaboration (LENPIC) project and was supported by the Polish National Science Center under Grants No. 2016/22/M/ST2/00173 and 2016/21/D/ST2/01120. The numerical calculations were performed on the supercomputer cluster of the JSC, Jülich, Germany.

APPENDIX: ELASTIC SCATTERING TRANSITION AMPLITUDE—*PT* TERM

The contribution to the elastic scattering transition amplitude $\langle\phi'|PT|\phi\rangle$ is given by [15,17]

$$\langle\phi'|PT|\phi\rangle = \sum_{JM}\sum_{\alpha' l_0\lambda_0 I_0}\left\langle 1m'_{s_0} I_0 M - m'_{s_0}\middle| JM\right\rangle\left\langle \lambda_0 M - m'_{s_0} - \mu'\frac{1}{2}\mu'\middle| I_0 M - m'_{s_0}\right\rangle$$
$$\times Y^*_{\lambda_0 M - m'_{s_0} - \mu'}(\hat{\tilde{q}})\int q'^2 dq'\int_{-1}^{1} dx\varphi_{l_0}(\pi_1)\frac{G_{\alpha_0,\alpha'}(q_0 q' x)}{\pi_1^{l_0}\pi_2^{l_{\alpha'}}}\langle\pi_2 q'\alpha'|T|\phi\rangle\,, \tag{A1}$$

where m'_{s_0} and μ' are spin projections of the outgoing deuteron and neutron in the final nd state ϕ' with relative momentum $\vec{\tilde{q}}$ ($|\vec{\tilde{q}}| = q_0$). The quantum numbers of the partial waves for given total angular momentum J (with projection M on the z axis defined by the incoming neutron momentum) and parity $\pi = (-1)^{l+\lambda}$ of the $3N$ system are given by $\alpha = [(ls)j(\lambda\frac{1}{2})I(jI)J(t\frac{1}{2}T)]$. The angular momentum l and spin s of the two-nucleon subsystem are coupled to its total angular momentum j and the total isospin is $t = 0$ or $t = 1$. The spectator nucleon orbital angular momentum λ coupled with its spin $\frac{1}{2}$ gives its total angular momentum I. The total isospin of the $3N$ system T results from coupling of t with spectator nucleon isospin $\frac{1}{2}$. The momentum π_1 in the deuteron wave function φ_{l_0} is given by $\pi_1 = \sqrt{q'^2 + \frac{1}{4}q_0^2 + q' q_0 x}$ while momentum $\pi_2 = \sqrt{q_0^2 + \frac{1}{4}q'^2 + q' q_0 x}$. The quantity $G_{\alpha_0,\alpha'}(q_0 q' x)/\pi_1^{l_0}\pi_2^{l_{\alpha'}}$ comes from the permutation operator P.

[1] H. Witala, W. Glöckle, D. Hüber, J. Golak, and H. Kamada, Phys. Rev. Lett. **81**, 1183 (1998).
[2] H. Witała, W. Glöckle, J. Golak, A. Nogga, H. Kamada, R. Skibiński, and J. Kuroś-Żołnierczuk, Phys. Rev. C **63**, 024007 (2001).
[3] N. Kalantar-Nayestanaki *et al.*, Rep. Prog. Phys. **75**, 016301 (2012).
[4] W. P. Abfalterer *et al.*, Phys. Rev. Lett. **81**, 57 (1998).
[5] H. Witała, H. Kamada, A. Nogga, W. Glöckle, Ch. Elster, and D. Hüber, Phys. Rev. C **59**, 3035 (1999).
[6] J. Kuroś-Żołnierczuk, H. Witała, J. Golak, H. Kamada, A. Nogga, R. Skibiński, and W. Glöckle, Phys. Rev. C **66**, 024003 (2002).
[7] S. A. Coon and H. K. Han, Few-Body Syst. **30**, 131 (2001).
[8] B. S. Pudliner, V. R. Pandharipande, J. Carlson, S. C. Pieper, and R. B. Wiringa, Phys. Rev. C **56**, 1720 (1997).

[9] R. B. Wiringa, V. G. J. Stoks, and R. Schiavilla, Phys. Rev. C **51**, 38 (1995).
[10] R. Machleidt, Phys. Rev. C **63**, 024001 (2001).
[11] V. G. J. Stoks, R. A. M. Klomp, C. P. F. Terheggen, and J. J. de Swart, Phys. Rev. C **49**, 2950 (1994).
[12] H. Witała, J. Golak, W. Glöckle, and H. Kamada, Phys. Rev. C **71**, 054001 (2005).
[13] H. Witała, J. Golak, R. Skibiński, W. Glöckle, W. N. Polyzou, and H. Kamada, Phys. Rev. C **77**, 034004 (2008).
[14] H. Witała, T. Cornelius, and W. Glöckle, Few-Body Syst. **3**, 123 (1988).
[15] W. Glöckle, H. Witała, D. Hüber, H. Kamada, and J. Golak, Phys. Rep. **274**, 107 (1996).
[16] D. Hüber, H. Kamada, H. Witała, and W. Glöckle, Acta Phys. Pol. B **28**, 1677 (1997).
[17] W. Glöckle, *The Quantum Mechanical Few-Body Problem* (Springer-Verlag, Berlin, 1983).
[18] S. A. Coon and M. T. Peña, Phys. Rev. C **48**, 2559 (1993).
[19] E. Epelbaum, A. Nogga, W. Glöckle, H. Kamada, Ulf-G. Meißner, and H. Witała, Phys. Rev. C **66**, 064001 (2002).
[20] V. Bernard, E. Epelbaum, H. Krebs, and Ulf-G. Meißner, Phys. Rev. C **77**, 064004 (2008).
[21] V. Bernard, E. Epelbaum, H. Krebs, and Ulf-G. Meißner, Phys. Rev. C **84**, 054001 (2011).
[22] M. Piarulli *et al.*, Phys. Rev. Lett. **120**, 052503 (2018).
[23] L. Girlanda, A. Kievsky, M. Viviani, and L. E. Marcucci, Phys. Rev. C **99**, 054003 (2019).